Proc. Int. Cong. of Math. – 2018
Rio de Janeiro, Vol. 3 (3473–3498)

CONVECTION-DIFFUSION-REACTION AND TRANSPORT-FLOW PROBLEMS MOTIVATED BY MODELS OF SEDIMENTATION: SOME RECENT ADVANCES

Raimund Bürger, Julio Careaga, Stefan Diehl, Camilo Mejías and Ricardo Ruiz Baier

Abstract

The sedimentation of a suspension is a unit operation widely used in mineral processing, chemical engineering, wastewater treatment, and other industrial applications. Mathematical models that describe these processes and may be employed for simulation, design and control are usually given as nonlinear, time-dependent partial differential equations that in one space dimension include strongly degenerate convection-diffusion-reaction equations with discontinuous coefficients, and in two or more dimensions, coupled flow-transport problems. These models incorporate non-standard properties that have motivated original research in applied mathematics and numerical analysis. This contribution summarizes recent advances, and presents original numerical results, for three different topics of research: a novel method of flux identification for a scalar conservation law from observation of curved shock trajectories that can be observed in sedimentation in a cone; a new description of continuous sedimentation with reactions including transport and reactions of biological components; and the numerical solution of a multi-dimensional sedimentation-consolidation system by an augmented mixed-primal method, including an a posteriori error estimation.

1 Introduction

1.1 Scope. The sedimentation of small particles dispersed in a viscous fluid under the influence of a (mostly gravitational) body force is a process of theoretical and practical interest that appears as a controlled unit operation in mineral processing, wastewater treatment, the pulp-and-paper and chemical industry, medicine, volcanology, and other areas

R.B. is supported by Conicyt (Chile) through Fondecyt project 1170473; BASAL project PFB03 CMM, U. de Chile and CI^{2}MA, U. de Concepción; and CRHIAM, project CONICYT/FONDAP/15130015. C.M. is supported by Conicyt scholarship. R.R.B. is supported by Engineering and Physical Sciences Research Council (EPSRC) through the grant EP/R00207X/1.

MSC2010: primary 35L65; secondary 76T20, 35Q35, 65M60, 65M08.

where a suspension must be separated into a clarified liquid and concentrated sediment. The authors are involved in the development and the mathematical and numerical analysis of models that describe these processes and may be employed for simulation and control in industrial applications. This contribution provides a survey of some recent advances in this area, which is related to nonlinear, time-dependent partial differential equations (PDEs).

1.2 Two-phase flow models of sedimentation. Sedimentation models for these applications should predict the behaviour of a given unit on relatively large temporal and spatial scales, while microscopical information such as the position of a given particle is of little interest. These considerations justify representing the liquid and the solid particles as superimposed continuous phases, namely a liquid phase and one or several solid phases. Since gravity acts in one dimension and computational resources for simulations are limited, spatially one-dimensional models are common. The continuous sedimentation of a suspension subject to applied feed and bulk flows, hindered settling and sediment compressibility can be modelled by a nonlinear, strongly degenerate parabolic PDE for the solids concentration $\phi = \phi(z,t)$ as a function of depth z and time t (Bürger, Karlsen, and Towers [2005]). This PDE is based on the solid and liquid mass balances, and its coefficients depend discontinuously on z.

To introduce the two-phase flow setting, we let ϕ denote the total solids volume fraction and $\boldsymbol{v}_\mathrm{s}$ and $\boldsymbol{v}_\mathrm{f}$ the solids and fluid phase velocity, respectively. Moreover, $\boldsymbol{v}_\mathrm{r} := \boldsymbol{v}_\mathrm{s} - \boldsymbol{v}_\mathrm{f}$ and $\boldsymbol{q} := \phi\boldsymbol{v}_\mathrm{s} + (1-\phi)\boldsymbol{v}_\mathrm{f}$ are the solid-fluid relative velocity (or drift velocity) and the volume average velocity of the mixture, respectively. Then the conservation of mass equations for the solid and the mixture can be written as

$$\partial_t \phi + \nabla \cdot \big(\phi \boldsymbol{q} + \phi(1-\phi)\boldsymbol{v}_\mathrm{r}\big) = 0, \quad \nabla \cdot \boldsymbol{q} = 0. \tag{1-1}$$

A constitutive assumption is introduced to specify $\boldsymbol{v}_\mathrm{r}$ (see below). In one space dimension, the model (1-1) is closed with q (i.e., $\boldsymbol{q}$ in one dimension) given by feed input as a function of t and by operating input and output flows as a piecewise constant function of z, while in two or three space dimensions, additional equations such as the Navier-Stokes equations need to be solved for the components of $\boldsymbol{q}$. In one space dimension, the simplest complete model is based on the kinematic assumption Kynch [1952] that v_r is a given function of ϕ, or equivalently, that the hindered settling function $v_\mathrm{hs}(\phi) = (1-\phi)v_\mathrm{r}(\phi)$ is given. Then the evolution of ϕ in a column is given by the scalar conservation law

$$\partial_t \phi - \partial_x f(\phi) = 0, \qquad 0 < x < 1, \tag{1-2}$$

with the nonlinear batch flux density function (Kynch [ibid.])

$$f(\phi) = \phi v_\mathrm{hs}(\phi). \tag{1-3}$$

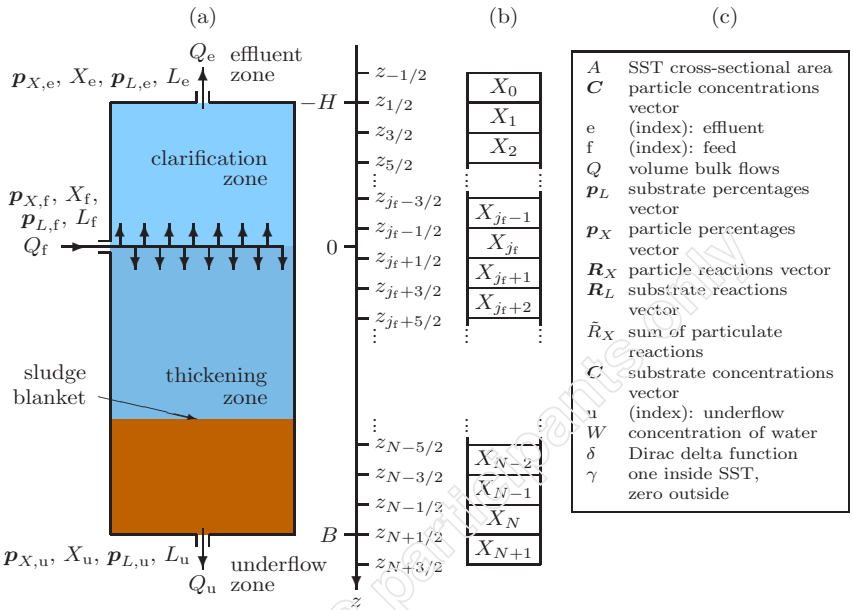

Figure 1: (a) An ideal secondary settling tank (SST) with variables of the feed inlet, effluent and underflow indexed with f, e and u, respectively (Bürger, Diehl, and Mejías [n.d.]). The sludge blanket (concentration discontinuity) separates the hindered settling and compression regions. (b) Subdivision into computational cells. (c) Nomenclature.

Here, x denotes height, $x = 0$ is the bottom of the column, and $x = 1$ the meniscus of the suspension. The initial and boundary conditions are $\phi(x,0) = \phi_0$ for $x \in (0,1)$, and $\phi(0^+,t) = 1$ and $\phi(1^-,t) = 0$ for $t > 0$. If f has exactly one inflection point, this problem has three different qualitative solutions, depending on the value of ϕ_0 (see Bürger and Diehl [2013]). Recent references to the background of (1-2), (1-3) include Betancourt, Bürger, Ruiz-Baier, Torres, and Vega [2014] and Diehl [2012].

1.3 A model PDE with rough coefficients. Continuous sedimentation is the process where gravity settling occurs in a large tank which is continuously fed with a suspension and from which a clarified liquid at the top and a thickened slurry at the bottom are withdrawn. For a tank with constant cross-sectional area this process can in one spatial dimension be modelled by the following PDE:

$$\partial_t \phi + \partial_z F(\phi, z, t) = \partial_z \big(\gamma(z) \partial_z D(\phi)\big) + s(t)\delta(z). \tag{1-4}$$

Here, the total flux function $F(\phi,z,t) = q(z,t)\phi + \gamma(z)f(\phi)$ contains the piecewise constant bulk velocity $q(\cdot,t)$, which has a discontinuity at the feed inlet depth $z = 0$. The source term is the product of the suspension feed flux $s(t)$ and the delta distribution $\delta(z)$. The characteristic function γ equals 1 inside the tank and 0 outside. Hence, $F(\phi,\cdot,t)$ has three discontinuities, namely at $z = 0$ and at the bottom ($z = B$) and top ($z = -H$) of the SST (Figure 1). The batch flux density function is given by (1-3) where v_{hs} can be given by the Richardson-Zaki expression

$$v_{\mathrm{hs}}(\phi) = v_0(1-\phi)^{n_{\mathrm{RZ}}}, \quad n_{\mathrm{RZ}} \geq 2, \tag{1-5}$$

by the Vesilind expression $v_{\mathrm{hs}}(\phi) = v_0 \exp(-r_{\mathrm{V}}\phi)$, $r_{\mathrm{V}} > 0$, or its correction

$$v_{\mathrm{hs}}(\phi) = v_0\big(\exp(-r_{\mathrm{V}}\phi) - \exp(-r_{\mathrm{V}}\phi_{\max})\big), \quad r_{\mathrm{V}} > 0, \tag{1-6}$$

or the formula (Diehl [2015])

$$v_{\mathrm{hs}}(\phi) = v_0/\big(1 + (\phi/\bar{\phi})^r\big), \quad \bar{\phi}, r > 0, \tag{1-7}$$

where $v_0 > 0$ is a constant that in (1-5) and (1-7) denotes the settling velocity of single particle in unbounded fluid, and $\phi_{\max}$ in (1-6) denotes a maximum solids concentration (see Diehl [ibid.] for references). Moreover, sediment compressibility is modeled by the degenerating diffusion term that involves the integrated diffusion coefficient

$$D(\phi) = \int_0^{\phi} \frac{\rho_X v_{\mathrm{hs}}(s)\sigma_{\mathrm{e}}'(s)}{g(\rho_X - \rho_L)}\,\mathrm{d}s, \tag{1-8}$$

where ρ_X and ρ_L denote the constant solid and fluid mass densities and σ_{e}' is the derivative of the so-called effective solid stress function $\sigma_{\mathrm{e}} = \sigma_{\mathrm{e}}(\phi)$ that satisfies

$$\sigma_{\mathrm{e}}'(\phi) = \frac{\mathrm{d}\sigma_{\mathrm{e}}(\phi)}{\mathrm{d}\phi} = \begin{cases} = 0 & \text{for } \phi \leq \phi_{\mathrm{c}}, \\ > 0 & \text{for } \phi > \phi_{\mathrm{c}}, \end{cases} \tag{1-9}$$

where ϕ_{c} denotes a critical concentration above which solid particles are assumed to form a porous network capable of supporting solid stress.

The well-posedness of the model described herein was established and numerical schemes were developed in Bürger, Karlsen, and Towers [2005]. It has meanwhile been extended in various directions, including reactive settling (Bürger, Careaga, Diehl, Mejías, Nopens, Torfs, and Vanrolleghem [2016] and Bürger, Diehl, and Mejías [n.d.]; see Section 3). Its usefulness for practical simulations (Bürger, Diehl, and Nopens [2011]), however, depends critically on that one can reliably identify the material specific model functions f and σ_{e} for the given material. The function f is usually identified via a batch settling experiment in a cylindrical vessel, but as we show in Section 2, this can be done more efficiently by a settling test in a cone.

1.4 A multi-dimensional model of sedimentation. In Section 4 we turn to the description of sedimentation processes in a multidimensional setting. We assume that the viscous fluid is incompressible so its mass and momentum balances are governed by the Navier-Stokes equations with variable viscosity, and the mass balance of the solid phase is described by a nonlinear advection-diffusion equation. Consequently, while in one space dimension one needs to solve only one scalar PDE such as (1-4) for the solids volume fraction ϕ, in several space dimensions we are faced with a system of PDEs that form coupled transport-flow problem for the computation of ϕ, the velocity field $\boldsymbol{q}$, and a pressure p.

The mathematical difficulties associated with such a problem include highly nonlinear (and typically degenerate) advection and diffusion terms, strong interaction of the $\boldsymbol{q}$ and ϕ fields via the Cauchy stress tensor and the forcing term, nonlinear structure of the overall coupled flow-transport problem, saddle-point structure of the flow problem, and non-homogeneous and mixed boundary conditions. These complications affect the solvability analysis of the model, the construction of numerical schemes, and the derivation of stability results and error bounds.

We are also interested in the construction of accurate, robust and reliable methods for the discretization of the model equations, and special emphasis is placed in primal-mixed finite element formulations, meaning that at both continuous and discrete levels, the flow equations possess a saddle-point structure involving the Cauchy stress as additional unknown, whereas the formulation of the advection-diffusion equation is written exclusively in terms of the primal variable, in this case ϕ. Such a structure yields stress approximations without postprocessing them from a low-order discrete velocity (which may lead to insufficiently reliable approximations). In Section 4 we review some recent developments on these lines.

2 Flux identification via curved shock trajectories

2.1 Model of sedimentation in a vessel with varying cross-sectional area. The batch settling of a suspension of initial concentration ϕ_0 in a vessel that occupies the height interval $x \in [0,1]$ and that at height x has the cross-sectional area $A(x)$ can be described by the initial-boundary value problem

$$\begin{aligned} &\partial_t\big(A(x)\phi\big) - \partial_x\big(A(x)f(\phi)\big) = 0, \quad 0 < x < 1, \quad t > 0; \\ &\phi(x,0) = \phi_0, \quad 0 < x < 1; \quad \phi(0^+,t) = \phi_{\max} = 1, \quad \phi(1^-,t) = 0, \quad t > 0, \end{aligned} \tag{2-1}$$

where we assume that $0 \le f \in C^2$ such that $f(0) = f(1) = 0$, with a single maximum at $\hat{\phi}$ and an inflexion point $\phi_{\text{infl}} \in (\hat{\phi}, 1]$, such that $f''(\phi) < 0$ for $\phi < \phi_{\text{infl}}$ and $f''(\phi) > 0$ for $\phi > \phi_{\text{infl}}$. Furthermore, we assume that $A(x)$ is invertible with $A'(x) \ge 0$.

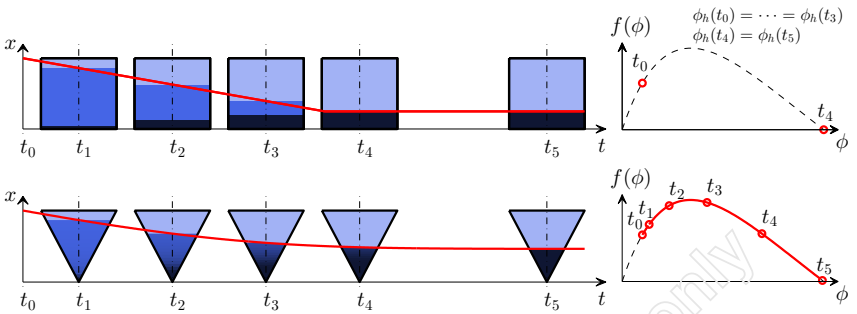

Figure 2: Schematic of settling of a suspension in a cylinder (top) and in a cone (bottom).

Specifically, we assume that

$$A(x) = \left(\frac{p + qx}{p + q} \right)^{1/q} \quad \text{for } 0 \le x \le 1 \tag{2-2}$$

for constants $p \ge 0$ and $q \ge 0$ ($p^2 + q^2 \neq 0$). Of particular interest is the case $p = 0$ and $q = 1/2$ that corresponds to a full cone, while $p > 0$ and $q = 1/2$ refers to a truncated cone. Cones are widely used for routine tests in sanitary engineering, where they are known as "Imhoff cones" (Bürger, Careaga, Diehl, Merckel, and Zambrano [n.d.]). The recent contribution by Bürger, Careaga, and Diehl [2017] related to (2-1) is the construction of explicit solutions to this problem. The basic difficulty associated with (2-1) is that characteristic curves and iso-concentration lines do not coincide. Furthermore, our solution handles functions f that have one inflection point, while the solution to (2-1) by Anestis [1981] was reduced to $f(\phi) = \phi(1 - \phi)$.

The practical interest in solving (2-1) for settling in a cone is illustrated in Figure 2: it turns out that in the conical case, the concentration ϕ beneath the suspension-supernate interface gradually increases, so that the velocity of descent of that interface decreases, while in the cylindrical case that concentration and velocity are constant. As a consequence, that velocity of descent depends on a whole interval of ϕ-values and corresponding flux values $f(\phi)$. It is therefore possible to reconstruct the function $\phi \mapsto f(\phi)$ on a whole interval, which may be as large as $(\phi_0, \phi_{\max}]$, where ϕ_0 is the initial concentration, from a single batch test, while the cylindrical case permits only to obtain one point $(\phi_0, f(\phi_0))$ in addition to $(\phi_{\max}, f(\phi_{\max}))$, so a separate test has to be performed for each initial concentration.

2.2 Solution of the initial-boundary value problem. The reconstruction is achieved through the exact solution of (2-1) by the method of characteristics wherever ϕ is smooth, combined with the solution of the ordinary differential equations for the suspension height h as a function of time t. The method of characteristics (see Holden and Risebro [2015]), applied to the PDE in (2-1) written in quasilinear form $\partial_t \phi - f'(\phi)\partial_x \phi = (A'(x)/A(x))f(\phi)$, yields that we may choose t as a parameter along characteristics, and that for a non-characteristic initial curve $(x,t,\phi) = (\xi,\tau,\varphi)$, the quantities $x = X(t)$ and $\phi = \Phi(t)$ satisfy the characteristic equations

$$\begin{aligned} X'(t) &= -f'(\Phi), \quad t > \tau; & \Phi'(t) &= \big(A'(X)/A(X)\big) f(\Phi), \quad t > \tau; \\ X(\tau) &= \xi, & \Phi(\tau) &= \varphi, \end{aligned}$$

from which we already read off that $A' > 0$ implies $\Phi' > 0$, i.e. the concentration increases along characteristics. For A given by (2-2) we get the characteristic system

$$\frac{t-\tau}{p+qx} = f(q)\int_{\varphi}^{\phi} \frac{\mathrm{d}\Phi}{f(\Phi)^{1+q}}, \qquad \frac{f(\phi)}{f(\varphi)} = \left(\frac{p+q\xi}{p+qx}\right)^{1/q}. \tag{2-3}$$

For $\varphi = \phi_0$ specified at initial time $\tau = 0$, the first equation in (2-3) yields

$$\psi(x,t) := \frac{t}{p+qx} = f(\phi)^q \int_{\phi_0}^{\phi} \frac{\mathrm{d}\Phi}{f(\Phi)^{1+q}} =: Q(\phi). \tag{2-4}$$

Thus, the solution $\phi = \phi(x,t)$ for small times is implicitly given by the relation

$$\psi(x,t) = Q(\phi), \tag{2-5}$$

where Q is invertible in closed form only in exceptional cases. However, (2-5) informs that the curves of constancy of ψ in an x versus t plot are those of ϕ, and for a (truncated) cone ($q = 1/2$), these are straight lines that intersect at $x = -p/q$.

The integral in (2-4) cannot be evaluated in closed form in general, but this is possible for the following case treated in Anestis [1981]:

$$f(\phi) = \phi(1 - \phi/\phi_{\max}), \quad q = 1/2. \tag{2-6}$$

Here we emphasize that our treatment (Bürger, Careaga, and Diehl [2017]) is based on integrals with respect to ϕ, while that of Anestis [1981] is based on integrating over values of f. This is the key insight that allowed us to handle flux functions having an inflection point.

Of course it is well known that the projected characteristics $t \mapsto x(t)$ for a quasilinear first-order PDE may intersect after finite time and give rise to discontinuities. If

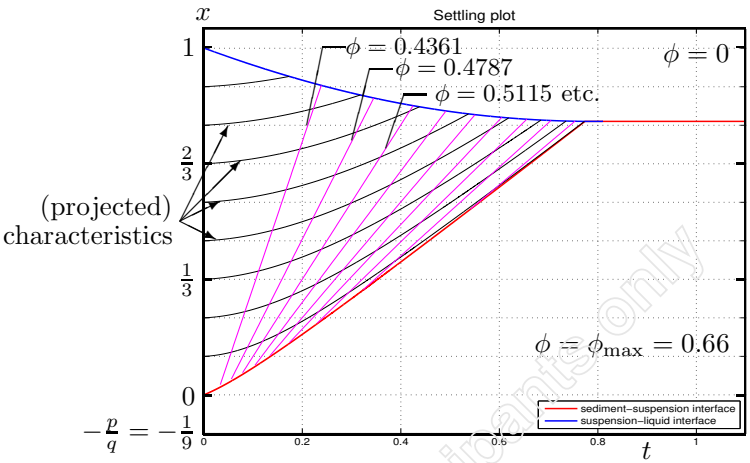

Figure 3: Construction of the entropy solution of (2-1) for (2-6) with $\phi_{\max} = 0.66$, $\phi_0 = 0.35$, and a truncated cone with $p = 1/18$.

$\phi^+(t) \neq \phi^-(t)$ are solution values adjacent to a curve $t \mapsto x_{\mathrm{d}}(t)$, then these must satisfy the Rankine-Hugoniot condition

$$-x_{\mathrm{d}}' = S(\phi^-, \phi^+) := (f(\phi^+) - f(\phi^-))/(\phi^+ - \phi^-) \tag{2-7}$$

and the entropy jump condition

$$S(u, \phi^-) \geq S(\phi^+, \phi^-) \text{ for all } u \text{ between } \phi^+ \text{ and } \phi^-. \tag{2-8}$$

Definition 2.1. *A function ϕ is an* entropy solution *of* (2-1) *if ϕ is a C^1 solution of* (2-1) *everywhere with the exception of a finite number of curves $x_{\mathrm{d}}(t) \in C^1$ of discontinuities. At each jump, $\phi^{\pm} := \phi(x_{\mathrm{d}}(t)^{\pm}, t)$ satisfy* (2-7) *and* (2-8).

Our approach is based on piecing together solutions $\phi = \phi(x,t)$ in smooth regions, where these are defined by (2-3), along with trajectories of discontinuities that satisfy (2-7) and (2-8). The entropy solution defined here is also the unique entropy solution in the sense of Kružkov-type entropy inequalities (Holden and Risebro [2015]). Such a solution may be used to provide exact reference solutions to test numerical schemes.

We illustrate in Figure 3 the construction for the case (2-6), for which the integral in (2-4) is available in closed form and Q is invertible, as considered in Anestis [1981]. The characteristics are upwards-bent curves, and the straight lines $\psi = $ const. intersect at

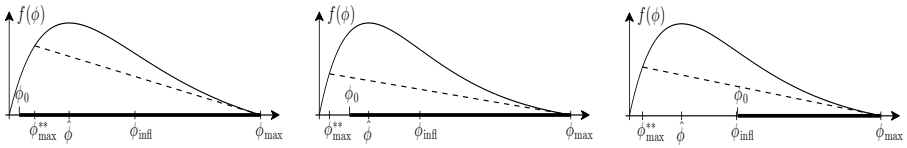

Figure 4: Generic cases of a low (L), medium (M), and high (H) value of ϕ_0. The thick lines show the intervals of possible identification of the flux.

$x = -p/q = -1/9$. These lines carry ϕ-values ranging from $\phi_0 = 0.35$ to $\phi_{\max} = 0.66$. The characteristic area is enclosed by two convex curves that separate the suspension from the clear liquid region ($\phi = 0$) and the sediment ($\phi = \phi_{\max}$) from the suspension, and which intersect at some time to form a stationary solution.

The construction of an entropy solution for a function f having an inflection point is more involved; see Bürger, Careaga, and Diehl [2017, n.d.] for full details. We here only provide those preliminaries that permit stating the final results in self-contained form.

To classify the generic cases that may arise for a function f with exactly one inflection point ϕ_{infl}, we introduce the operations $\phi \mapsto \phi^*$ and $\phi \mapsto \phi^{**}$:

$$\phi^* := \sup\{u > \phi : S(\phi, u) \le S(\phi, v)\ \forall v \in (\phi, u]\} \quad \text{for } \phi \in [0, \phi_{\text{infl}}],$$
$$\phi^{**} := \inf\{u < \phi : u^* = \phi\} \quad \text{for } \phi \in [\phi_{\text{infl}}, \phi_{\max}].$$

The generic cases are then those of a low (L), medium (M), and high (H) value of ϕ_0 in terms of comparisons with ϕ_{infl} and $\phi^{**}_{\max}$, see Figure 4.

Let us first consider a truncated cone ($q = 1/2$, $p > 0$). The solutions are illustrated in Figure 5. In each case an upper discontinuity $x = h(t)$ is defined for $0 \le t \le t_3$, where t_3 is the time at which the solution becomes stationary, and in Cases L and M a lower discontinuity $x = b(t)$ emerges from $x = 0$ at $t = t_1 > 0$, and may cease to exist at a time t_2 or merge with $h(t)$ at $t = t_{2.5}$. Regions I, IIa, etc. (denoted R_{I}, R_{IIa}, etc.) contain qualitatively different smooth solutions. The following theorem is proved in Bürger, Careaga, and Diehl [2017].

Theorem 2.1. *Assume that A is given by (2-2) with $p, q > 0$ or $p > 0$ and $q \to 0^+$. Then the entropy solution $\phi = \phi(x,t)$ of (2-1) is piecewise smooth and has a descending shock $h(t)$, which is strictly convex for $0 < t < t_3$. Moreover:*

(i) A discontinuity $b(t)$ rises from $x = 0$ if and only if $0 < \phi_0 < \phi_{\text{infl}}$ (Cases L and M). It is a shock for $0 \le t < t_1$, a contact for $t_1 \le t < t_2$, and strictly convex for $0 \le t < t_2$. Here h and b are smooth, except if $t_2 = t_{2.5}$ (i.e., h and b intersect); then h' jumps at $t = t_{2.5}$. If $t_2 < t_{2.5}$, then $b(t)$ dies at $t = t_2$.

(ii) $\partial_t \phi > 0$ *and* $\partial_x \phi < 0$ *(weakly) except for* $\phi = 0$ *for* $x > h(t)$ *and* $\phi = \phi_{\max}$ *in* R_{III}*; and if* $q = 0$*, then* $\partial_t \phi > 0$ *and* $\partial_x \phi = 0$ *in* R_{I}.

(iii) In R_{I}, $\phi(x,t) = Q^{-1}(\psi(x,t))$.

(iv) $R_{\mathrm{IIa}} = \varnothing$ *if* $\phi_{\mathrm{infl}} \leq \phi_0 < \phi_{\max}$ *(Case H) or if* $P(\phi_{\mathrm{infl}}) \leq 0$ *and* $\phi_G < \phi_0 < \phi_{\mathrm{infl}}$*. Otherwise,* $\phi > \phi_{\mathrm{infl}}$ *in* R_{IIa}*, and strictly concave characteristics emanate tangentially from* $b(t)$ *for* $t_1 \leq t \leq t_2$.

(v) $R_{\mathrm{IIb}} = \varnothing$ *if* $\phi_0 \leq \phi^{**}_{\max}$ *(Case L). Otherwise* R_{IIb} *is filled with concave characteristics emanating from* $(x,t) = (0,0)$ *with initial values in* $(\phi^{*}_{0}, \phi_{\max})$ *in Case M, and in* $(\phi_0, \phi_{\max})$ *in Case H.*

Note that Theorem 2.1 does not cover the case of a full cone, that is, $q = 1/2$ and $p = 0$. In fact, it is not entirely straightforward to take the limit $p \to 0^+$ in the proof of Bürger, Careaga, and Diehl [2017] since a singularity arises at $(x,t) = (0,0)$ even if no singularity is created for $p > 0$. For the identification problem, the case $p = 0$ is of interest since full cones are common laboratory equipment, and more importantly, for the following reason. The conversion of the curve $(t, h(t))$ into a portion of the flux, that is, into pairs $(\phi, f(\phi))$ on a certain ϕ-interval is possible for $0 \leq t \leq t_{2.5}$ Bürger, Careaga, and Diehl [2017, n.d.]. However, the time $t_{2.5}$, that is the moment of merger of $b(t)$ and $h(t)$, may be hard to be detect. Fortunately, for $p = 0$ it turns out that $t_{2.5} = t_3$ (under some mild conditions), and therefore the entire curve $h(t)$ may be used for all times for flux identification. The following theorem is proved in Bürger, Careaga, and Diehl [n.d.].

Theorem 2.2. *Assume that* A *is given by* (2-2) *with* $p = 0$ *and* $q > 0$*. The entropy solution* $\phi = \phi(x,t)$ *of* (2-1) *is piecewise smooth and satisfies (i) and (ii) of Theorem 2.1. If* $f'(\phi_{\max}) < 0$*, then* $t_3 < \infty$ *and* $\phi \equiv \phi_{\max}$ *in* R_{III}*, which is bounded by the upper shock curve* $x = h(t)$ *and the line* $x = \ell(t) := -f'(\phi_{\max})t$*. If* $f'(\phi_{\max}) = 0$*, then* $R_{\mathrm{III}} = \varnothing$*. Furthermore, we define* $P(\phi) := \frac{Q'(\phi)}{q f(\phi)^{q-1}}$*, and have the following.*

(i) Independently of ϕ_0*: If* $P(\phi_{\mathrm{infl}}) > 0$*, then the solution is continuous in* $0 \leq x \leq h(t)$*,* $t > 0$*, without a bottom discontinuity* $b(t)$*. (See Figure 6.)*

(ii) If $\phi_0 \leq \phi_{\mathrm{infl}}$ *(Cases L and M) and* $P(\phi_{\mathrm{infl}}) \leq 0$*, then the solution has both discontinuities, where* $b(t)$ *is a straight line originating from the bottom, having the constant* $\phi = \phi_{\mathrm{G}}$ *just above it, where* $G(\phi_{\mathrm{G}}) = 0$ *and we define the function* $G(\varphi) := S(\varphi, \varphi^-) + \frac{1}{qQ(\varphi)}$.

2.3 Solution of the inverse problem and curved trajectories. Let us now come back to the inverse problem. We assume that $A(x)$ is given by (2-2) with $p, q \geq 0$, that the intial

concentration ϕ_0 is given, and that the flux is unknown but has the following properties: $f \in C^2$ is a nonnegative function with $f(0) = f(1) = 0$, one maximum $\hat{\phi}$ and one inflection point $\phi_{\text{infl}} \in (\hat{\phi}, 1]$ such that $f''(\phi) < 0$ for $\phi < \phi_{\text{infl}}$ and $f''(\phi) > 0$ for $\phi > \phi_{\text{infl}}$. Then the inverse problem can be formulated as follows (see Figure 2):

(IP) *Given the interface trajectory* $[t_{\text{start}}, t_{\text{end}}] \ni t \mapsto h(t)$, *find the portion of* $\phi \mapsto f(\phi)$ *corresponding to the interval of adjacent* ϕ*-values.*

The idea to solve (IP) is based on the representation of the explicit solution according to Theorems 2.1 and 2.2. In Bürger, Careaga, and Diehl [ibid.] the solution of (IP) is given as a parametric explicit formula for the flux. If $h(t)$ is not provided in closed algebraic form, for instance if only pointwise experimental data are available, then a suitable decreasing and convex approximation can be generated by solving a constrained least-squares approximation (quadratic programming) problem; see Bürger, Careaga, and Diehl [n.d.] and Bürger and Diehl [2013].

To elucidate a relation between curved shock trajectories and the functional form of the nonlinear flux, let us consider for the moment the cylindrical case $A \equiv$ const., for which the identification problem was handled in Bürger and Diehl [2013]. Then, the upper discontinuity $x = h(t)$ is initially a straight line; see Figure 2. For a medium large initial value $\phi_0 \in (\phi^{**}_{\max}, \phi_{\text{infl}})$, a rarefaction fan emerges from $(x,t) = (0,0)$. After this wave has met the upper discontinuity $h(t)$ at $t = t_{\text{start}}$, the latter becomes convex for some $t \in [t_{\text{start}}, t_{\text{end}}]$. Kynch [1952] presented a graphical procedure for obtaining f in the interval $[\phi^*_0, \phi_{\max}]$ (the 'tail'). Diehl [2007] showed that Kynch's graphical procedure can be written by representation formulas; namely the tail of f can be expressed as a function of the curved discontinuity h and its derivative h'. This is a solution of the inverse problem of obtaining (the tail of) the flux function f given the solution of (2-1) with $A \equiv$ const.. It is interesting to note that Kunik [1993] presented a representation formula for the global solution of (2-1) with $A \equiv$ const. for a monotone initial value function $\phi(x,0) = \phi_{\text{init}}(x)$, $0 \le x \le 1$. In the special batch-sedimentation case where $\phi_{\text{init}} \equiv \phi_0$, Kunik's formulas relate the curved discontinuity h as a function of the flux function f in precisely the same way as Diehl's formulas relate f as a function of h. To elucidate this symmetry, we denote the concentration just below the curved discontinuity by

$$\phi_h(t) := \phi(h(t)^-, t) \quad \text{for } t_{\text{start}} \le t \le t_{\text{end}}, \tag{2-9}$$

where ϕ_h is an increasing C^1 function that maps $[t_{\text{start}}, t_{\text{end}}]$ to $[\phi^*_0, \phi_{\max}]$. In the rest of this section, we restrict h and f to these respective intervals. Evaluating the formula $x/t = -f'(\phi(x,t))$, which describes the slope of characteristics within the rarefaction wave, and inserting (2-9) we obtain

$$h(t)/t = -f'(\phi_h(t)) \quad \text{for } t_{\text{start}} \le t \le t_{\text{end}}. \tag{2-10}$$

On the other hand, the jump condition (2-7) for $x = h(t)$ implies that

$$-h'(t) = f(\phi_h(t))/\phi_h(t) \quad \text{for } t_{\text{start}} \le t \le t_{\text{end}}. \tag{2-11}$$

Note that replacing h by f and t by ϕ_h in any of the formulas (2-10) and (2-11), the other is obtained. In fact, defining $\eta(t) := h(t) - th'(t)$ and $\tilde{\Phi}(\phi) := f(\phi) - \phi f'(\phi)$, we obtain the following dual representation formulas Bürger and Diehl [2013]:

$$\big(\phi, f(\phi)\big) = \big(H\phi_0/\eta(t)\big)\big(1, -h'(t)\big) \quad \text{for } t_{\text{start}} \le t \le t_{\text{end}}, \tag{2-12}$$

$$\big(t, h(t)\big) = \big(H\phi_0/\tilde{\Phi}(\phi)\big)\big(1, -f'(\phi)\big) \quad \text{for } H\phi_0/\eta(t_{\text{start}}) = \phi_0^* \le \phi \le \phi_{\max}, \tag{2-13}$$

where (2-12) was derived by Diehl [2007] and (2-13) by Kunik [1993]. Both f and h are decreasing, strictly convex and C^2 functions (on the intervals of interest). Since both η and $\tilde{\Phi}$ are invertible, explicit representation formulas may be obtained:

$$f(\phi) = -\phi h'\left(\eta^{-1}\left(H\phi_0/\phi\right)\right) \quad \text{for } \phi_0^* \le \phi \le \phi_{\max},$$

$$h(t) = -tf'\left(\tilde{\Phi}^{-1}(H\phi_0/t)\right) \quad \text{for } t_{\text{start}} \le t \le t_{\text{end}}.$$

2.4 A numerical example. We are currently applying the new method of flux identification to synthetic and experimental data (Bürger, Careaga, Diehl, Merckel, and Zambrano [n.d.]). We show in Figure 1 the numerical solution to a problem of flux recognition. The flux function $f(\phi)$ defined by (1-3) and (1-6) with $r_{\text{V}} = 5$ was used to produce the upper discontinuity by solving the corresponding jump condition ODE numerically. From the ODE solution, discrete data points were obtained and used to fit a piecewise cubic polynomial function $h(t)$. This function is then used in the explicit parametric formula (see Bürger, Careaga, and Diehl [n.d.]) for the flux. With sufficiently many data points, containing hardly any noise, many subintervals can be used and a portion of the flux identified accurately.

3 Reactive settling

3.1 Introduction. Models of continuously operated settling tanks form a topic for well-posedness and numerical analysis even in one space dimension due to the spatially discontinuous coefficients of the underlying strongly degenerate parabolic, nonlinear model PDE (1-4). Such a model was recently extended (Bürger, Careaga, Diehl, Mejías, Nopens, Torfs, and Vanrolleghem [2016] and Bürger, Diehl, and Mejías [n.d.]) to multi-component particles that react with several soluble constituents of the liquid phase. The fundamental balance equations contain the mass percentages of the components of both phases. The

equations are reformulated in Bürger, Diehl, and Mejías [n.d.] as a system of nonlinear PDEs that can be solved by an explicit numerical difference scheme. The scheme itself is not described in this contribution since space is limited. It combines a difference scheme for conservation laws with discontinuous flux, similar to that of Bürger, Karlsen, and Towers [2005], with numerical percentage propagation for multi-component flows (Diehl [1997]).

3.2 Mathematical model. The main variables are explained in Figure 1. The unknowns are X, L, $\boldsymbol{p}_X$ and $\boldsymbol{p}_L$ as functions of z and t. The solid and fluid densities, ρ_X and ρ_L, are assumed constant. The model keeps track of k_X particulate and k_L liquid components ($k_L - 1$ substrates and water), whose concentrations are collected in vectors $\boldsymbol{C}$ and $\boldsymbol{S}$ along with W, or equivalently, percentage vectors $\boldsymbol{p}_X$ and $\boldsymbol{p}_L$:

$$\boldsymbol{C} = \boldsymbol{p}_X X = \begin{pmatrix} p_X^{(1)} \\ \vdots \\ p_X^{(k_X)} \end{pmatrix} X, \quad \boldsymbol{p}_L L = \begin{pmatrix} p_L^{(1)} \\ \vdots \\ p_L^{(k_L)} \end{pmatrix} L = \begin{pmatrix} \boldsymbol{S} \\ W \end{pmatrix} = \begin{pmatrix} S^{(1)} \\ \vdots \\ S^{(k_L-1)} \\ W \end{pmatrix},$$

where $p_X^{(1)} + \cdots + p_X^{(k_X)} = 1$ and $p_L^{(1)} + \cdots + p_L^{(k_L)} = 1$. The governing system of equations can be formulated as follows:

(3-1)

$$\partial_t X + \partial_z F_X = \delta(z)\frac{X_\mathrm{f} Q_\mathrm{f}}{A} + \gamma(z)\tilde{R}_X(X), \quad F_X := Xq + \gamma(z)\big(f(X) - \partial_z D(X)\big),$$

$$\partial_t(\boldsymbol{p}_X X) + \partial_z(\boldsymbol{p}_X X) = \delta(z)\frac{\boldsymbol{p}_{X,\mathrm{f}} X_\mathrm{f} Q_\mathrm{f}}{A} + \gamma(z)\boldsymbol{R}_X,$$

$$L = \rho_L(1 - X/\rho_X),$$

$$\partial_t(\bar{\boldsymbol{p}}_L L) + \partial_z(\bar{\boldsymbol{p}}_L L) = \delta(z)\frac{\bar{\boldsymbol{p}}_{L,\mathrm{f}} X_\mathrm{f} Q_\mathrm{f}}{A} + \gamma(z)\bar{\boldsymbol{R}}_L, \quad F_L := \rho_L\left(q - \frac{F_X}{\rho_X}\right),$$

$$p_L^{(k_L)} = 1 - \big(p_L^{(1)} + \cdots + p_L^{(k_L-1)}\big)$$

for $z \in \mathbb{R}$ and $t > 0$, along with suitable initial conditions. The convective flux function F_X contains the spatially discontinuous bulk velocity $q(z,t)$, the hindered-settling flux function f given by (1-3) and the sediment compressibility function D by (1-8). Moreover, $\bar{\boldsymbol{p}}_L = \bar{\boldsymbol{p}}_L(z,t)$ is a vector of components of the liquid phase formed by the first $k_L - 1$ components of $\boldsymbol{p}_L$. The reaction term vectors are denoted by $\boldsymbol{R}_X$ and $\bar{\boldsymbol{R}}_L$, and lastly $\tilde{R}_X$ is the sum of all components of the vector $\boldsymbol{R}_X$.

The model (3-1) may include a full biokinetic Activated Sludge Model (ASMx; see Henze, Grady, Gujer, Marais, and Matsuo [1987]) at every depth z within $\boldsymbol{R}_X$ and $\bar{\boldsymbol{R}}_L$,

and is based on the idea that hindered and compressive settling depend on the total particulate concentration (flocculated biomass) X modelled by the first equation. The particular formulation (3-1) has two advantages. Firstly, for a numerical method with explicit time stepping such as the one advanced in Bürger, Diehl, and Mejías [n.d.], the new value of X is obtained by solving the first equation in (3-1) only. Then $\boldsymbol{p}_X$ is updated by the second equation of (3-1), etc. Secondly, this formulation yields the invariant region property of the numerical scheme (see Bürger, Diehl, and Mejías [ibid., Theorem 4.1]), which states that the solution stays in

$$\tilde{\Omega} := \big\{\mathcal{U} \in \mathbb{R}^{k_X+k_L+2} : 0 \le \boldsymbol{p}_X, \boldsymbol{p}_L \le 1,\ 0 \le X \le X_{\max},\\ \rho_L - rX_{\max} \le L \le \rho_L,\ p_X^{(1)} + \cdots + p_X^{(k_X)} = 1,\ p_L^{(1)} + \cdots + p_L^{(k_L)} = 1\big\}$$

(vectors in inequalities should be interpreted component-wise), provided that the spatial meshwidth and the time step satisfy a suitable CFL condition.

We have no proof that an exact solution of system (3-1) stays in $\tilde{\Omega}$ if the initial datum does since the well-posedness (existence and uniqueness) analysis of the model is not yet concluded, and a suitable concept of a (discontinuous) exact solution is not yet established. However, it is reasonable to expect that an exact solution of (3-1) should also assume values within $\tilde{\Omega}$. To support this conjecture, we mention first that the invariant region property proved in Bürger, Diehl, and Mejías [ibid.] holds uniformly for approximate solutions, and therefore will hold for any limit to which the scheme converges as discretization parameters tend to zero. This standard argument has been used for related models in Bürger, Karlsen, Risebro, and Towers [2004], Bürger, Karlsen, and Towers [2005], and Karlsen, Risebro, and Towers [2002]. With the properties of the reaction term here, namely that $\tilde{R}_X = 0$ if $X = 0$ or $X = X_{\max}$, the invariance property of the numerical scheme follows by a monotonicity argument (Bürger, Diehl, and Mejías [n.d., Lemma 4.3]). The convergence of that scheme with a reaction term being a function of X only (and utilizing that it is zero for $X = 0$ or $X = X_{\max}$) can be established by modifying the proof in Bürger, Karlsen, and Towers [2005].

3.3 Numerical example. To specify the function f given by (1-3), we utilize (1-7) with volume fraction ϕ replaced by the equivalent local density X and the parameters $\bar{X} = 3.87\,\mathrm{kg\,m^{-3}}$ and $r = 3.58$. The function D that describes sediment compressibility is specified by (1-8), where we choose $\sigma_e = 0$ for $X < X_c$ and $\sigma_e(X) = \alpha(X - X_c)$ for $X > X_c$ with $\alpha = 0.2\,\mathrm{m^2\,s^{-2}}$ and $X_c = 5\,\mathrm{kg\,m^{-3}}$. The velocity q is defined in terms of the given bulk flows as

$$q(z,t) = \frac{1}{A} \cdot \begin{cases} Q_e(t) = Q_f(t) - Q_u(t) & \text{for } z < 0, \\ Q_u(t) & \text{for } z > 0, \end{cases} \qquad \text{where } A = 400\,\mathrm{m^2}.$$

We use a reduced biological model of denitrification, distinguishing $k_X = 2$ particulate components with concentrations X_{OHO} (ordinary heterotrophic organisms) and X_{U} (undegradable organics), and $k_L = 4$ liquid components, namely the substrates $S_{\mathrm{NO_3}}$ (nitrate), S_S (readily biodegradable substrate) and $S_{\mathrm{N_2}}$ (nitrogen), and water, such that $\boldsymbol{p}_X X = \boldsymbol{C} = (X_{\mathrm{OHO}}, X_{\mathrm{U}})^{\mathrm{T}}$ and $\boldsymbol{S} = (S_{\mathrm{NO_3}}, S_{\mathrm{S}}, S_{\mathrm{N_2}})^{\mathrm{T}}$. The reaction terms are then given by

$$\boldsymbol{R}_L = X_{\mathrm{OHO}} \begin{pmatrix} -\dfrac{1-Y}{2.86Y}\mu(\boldsymbol{S}) \\ (1-f_{\mathrm{p}})b - \dfrac{1}{Y}\mu(\boldsymbol{S}) \\ \dfrac{1-Y}{2.86Y}\mu(\boldsymbol{S}) \\ 0 \end{pmatrix}, \qquad \boldsymbol{R}_X = X_{\mathrm{OHO}} \begin{pmatrix} \mu(\boldsymbol{S}) - b \\ f_{\mathrm{p}} b \end{pmatrix},$$

$$\mu(\boldsymbol{S}) := \mu_{\max} \frac{S_{\mathrm{NO_3}}}{K_{\mathrm{NO_3}} + S_{\mathrm{NO_3}}} \frac{S_{\mathrm{S}}}{K_{\mathrm{S}} + S_{\mathrm{S}}},$$

where $\mu(\boldsymbol{S})$ is the so-called growth rate function. (Values of constants are given in the caption of Figure 9.) The resulting summed reaction terms are

$$\tilde{R}_X = (\mu(\boldsymbol{S}) - (1-f_{\mathrm{p}})b)\, X_{\mathrm{OHO}}, \quad \tilde{R}_L = \left((1-f_{\mathrm{p}})b - \frac{\mu(\boldsymbol{S})}{Y}\right) X_{\mathrm{OHO}}.$$

We choose the volumetric flows Q_{f} and Q_{u} and the feed concentration X_{f} as piecewise constant functions of t (see Figure 8), and let $\boldsymbol{p}_{X,\mathrm{f}}$ and $\boldsymbol{p}_{L,\mathrm{f}}$ be constant.

The whole simulation is shown in Figure 9. The initial steady state is kept during two hours of the simulation. There is a sludge blanket, i.e., a discontinuity from a low concentration up to $X = X_{\mathrm{c}}$. At $t = 4\,\mathrm{h}$, the step change of control functions causes a rapidly rising sludge blanket that nearly reaches the top of the SST around $t = 5.8\,\mathrm{h}$, when the control variables are changed again. The fast reactions imply that the soluble NO_3 is quickly converted to N_2 in regions where the bacteria OHO are present, which is below the sludge blanket.

4 A multi-dimensional sedimentation model

4.1 Coupled transport-flow problem. Consider an incompressible mixture occupying the domain $\Omega \subset \mathbb{R}^d$, $d = 2$ or $d = 3$, and that the velocities $\boldsymbol{q}$ and $\boldsymbol{v}_{\mathrm{r}}$ are as defined in Section 1.2. Following Bürger, Wendland, and Concha [2000] and discarding quadratic terms for the filtration velocity, we may recast the governing equations as follows (cf.

Ruiz-Baier and Lunati [2016]):

$$
\begin{aligned}
\operatorname{div} \boldsymbol{q} &= 0, \\
\partial_t \phi + \operatorname{div}(\phi \boldsymbol{q} - b(\phi)\boldsymbol{k}) &= \operatorname{div}(\kappa(\phi)\nabla\phi), \\
\partial_t \boldsymbol{q} + \boldsymbol{q}\cdot\nabla\boldsymbol{q} - \frac{1}{\rho}\mathbf{div}\big(\mu(\phi)\boldsymbol{\varepsilon}(\boldsymbol{q}) - p\boldsymbol{I}\big) &= \mathbb{Q}(\phi)(\partial_t \boldsymbol{v}_{\mathrm{r}} + \boldsymbol{q}\cdot\nabla\boldsymbol{v}_{\mathrm{r}}) \\
&\quad + \mathbb{Q}(\phi)\boldsymbol{v}_{\mathrm{r}}\cdot\nabla\boldsymbol{q} + g\boldsymbol{k},
\end{aligned}
\tag{4-1}
$$

where $\rho = \phi\rho_X + (1-\phi)\rho_L$ is the local density of the mixture, $\mathbb{Q}(\phi) = \rho^{-1}(\rho_X - \rho_L)\phi(1-\phi)$, and $b(\phi)$ is the Kynch batch flux density function, i.e., $b(\phi) = f(\phi)$ in the notation of Sections 1.2 and 1.3, where we assume that this function is given by (1-3), (1-5) with $n_{\mathrm{RZ}} = 0$. The coefficient functions $\kappa(\phi) := (\mathrm{d}D(\phi)/\mathrm{d}\phi)/\rho_X$ (see (1-8)) and $\mu(\phi) := (1-\phi)^{-3}$ account for compressibility of the sediment and mixture viscosity, respectively.

The primal unknowns are the volume average flow velocity of the mixture $\boldsymbol{q}$, the solids concentration ϕ, and the pressure field p. Next we proceed to recast (4-1) in mixed form, also making the assumption that the flow regime is laminar: Find the Cauchy fluid pseudo-stress $\boldsymbol{\sigma}$, the velocity $\boldsymbol{q}$, and the volume fraction ϕ satisfying

$$
\begin{aligned}
&(\mu(\phi))^{-1}\boldsymbol{\sigma}^{\mathrm{d}} = \nabla\boldsymbol{q}, \quad \partial_t\boldsymbol{q} - \mathbf{div}\,\boldsymbol{\sigma} = \boldsymbol{f}\phi, \quad \operatorname{div}\boldsymbol{q} = 0 \quad \text{in } \Omega, \\
&\widetilde{\boldsymbol{\sigma}} = \vartheta(\phi)\nabla\phi - \phi\boldsymbol{q} + b(\phi)\boldsymbol{k}, \quad \partial_t\phi - \operatorname{div}\widetilde{\boldsymbol{\sigma}} = g \quad \text{in } \Omega.
\end{aligned}
\tag{4-2}
$$

This system is supplemented with the following boundary conditions:

$$
\boldsymbol{q} = \boldsymbol{q}_{\mathrm{D}}, \quad \phi = \phi_{\mathrm{D}} \quad \text{on } \Gamma_{\mathrm{D}}; \quad \boldsymbol{\sigma}\boldsymbol{\nu} = \boldsymbol{0}, \quad \widetilde{\boldsymbol{\sigma}}\cdot\boldsymbol{\nu} = 0 \quad \text{on } \Gamma_{\mathrm{N}}
\tag{4-3}
$$

along with the initial data $\boldsymbol{q}(0) = \boldsymbol{q}_0$, $s(0) = s_0$ in $\Omega \times \{0\}$. Here $(\cdot)^{\mathrm{d}}$ denotes the deviatoric operator, $\boldsymbol{k}$ is a vector pointing in the direction of gravity and $\boldsymbol{f} \in \mathbf{L}^\infty(\Omega)$, $\boldsymbol{q}_{\mathrm{D}} \in \mathbf{H}^{1/2}(\Gamma_{\mathrm{D}})$, $g \in \mathrm{L}^2(\Omega)$ are given functions.

Even if problems with the ingredients mentioned above have successfully been simulated numerically by many techniques (see e.g. Betancourt, Bürger, Ruiz-Baier, Torres, and Vega [2014], Khalili, Basu, Pietrzyk, and Jørgensen [1999], Ekama, Barnard, Günthert, Krebs, McCorquodale, Parker, and Wahlberg [1997], and Rao, Mondy, and Altobelli [2007]), the study of mathematical properties of (4-1) and the rigorous analysis of discretizations is still an open problem in the general case. The parabolic regularization approach has been exploited in Bürger, Liu, and Wendland [2001] to address the well-posedness of (4-1) for a large fluid viscosity. Its formulation in terms of Stokes flow and the steady coupling to compression effects has been recently studied in Alvarez, Gatica, and Ruiz-Baier [2015]. That contribution assumes that the nonlinear diffusivity

depends on the concentration gradient, which is also done, for instance, for reacting non-Newtonian fluids Bulíček and Pustějovská [2014]. More general viscosity and diffusivity functions were analyzed in Alvarez, Gatica, and Ruiz-Baier [2016b], but still assuming non-degeneracy of the diffusion term. Models of sedimentation-consolidation are similar in structure to Boussinesq- and Oldroyd-type models, for which several mixed formulations have been analyzed (see Colmenares, Gatica, and Oyarzúa [2016], Farhloul and Zine [2011], and Cox, Lee, and Szurley [2007] and references cited in these papers). Augmentation of the formulation, as done in Alvarez, Gatica, and Ruiz-Baier [2015, 2016b], simplifies the analysis of continuous and discrete problems associated to (4-2)–(4-3).

4.2 Finite volume element schemes. The dominance of convection in the diffusive transport equation in (4-1) suggests the use of finite volume (FV)-based discretizations. In turn, finite element (FE) formulations are more suitable for error analysis by energy arguments and for setting up mixed formulations. Finite-volume-element (FVE) schemes retain properties of both FV and FE methods. Their construction hinges on defining fluxes across element boundaries defined on a dual partition of the domain (see Bank and Rose [1987] for details and Quarteroni and Ruiz-Baier [2011], Kumar and Ruiz-Baier [2015], and Wen, He, and Yang [2013] for recent applications in incompressible flows). Variants of FVE schemes have been employed for reactive flows (Ewing, Lazarov, and Lin [2000]), variable viscosity flows (Calgaro, Creusé, and Goudon [2008]), sedimentation equations in axisymmetric form and including mild (pointwise) degeneracy (Bürger, Ruiz-Baier, and Torres [2012]), incorporating convective terms and using a conforming approximation in primal form (Ruiz-Baier and Torres [2015]), defining discontinuous discretizations for velocity-pressure and concentration (Bürger, Kumar, and Ruiz-Baier [2015]), also in the case of porous materials (Bürger, Kumar, Kenettinkara, and Ruiz-Baier [2016]).

4.3 A posteriori error estimation. Mesh adaptivity guided by a posteriori error estimates has a considerable potential in sedimentation-consolidation problems. Exploiting intrinsic differences in spatio-temporal scales, adaptive methods have been developed for the 1D case (Bürger, Ruiz, Schneider, and Sepúlveda [2008]) using multiresolution techniques, whereas the a posteriori error analysis for general coupled viscous flow-transport problems has only been addressed in Alvarez, Gatica, and Ruiz-Baier [2016b], Braack and Richter [2007], and Larson, Söderlund, and Bengzon [2008], and Alvarez, Gatica, and Ruiz-Baier [2017] in a specific application to sedimentation processes in porous media. In Alvarez, Gatica, and Ruiz-Baier [ibid.] efficient and reliable residual-based a posteriori error estimators for augmented mixed–primal FE schemes for stationary versions of (4-2)–(4-3) are proposed, and a generalization to the transient case can be defined as described below.

Given an element of the FE mesh $K \in \mathcal{T}_h$, we denote by $\mathcal{E}_h(K)$ the set of its edges not sharing any boundary segments, and let $\mathcal{E}_h^{\Gamma_D}(K)$ denote the set of edges of K lying on the boundary Γ_D. The unit normal vector on each edge is $\boldsymbol{\nu}_e := (\nu_1, \nu_2)^T$, and let $\boldsymbol{s}_e := (-\nu_2, \nu_1)^T$ be the corresponding fixed unit tangential vector along e. We let $[\![\boldsymbol{v} \cdot \boldsymbol{\nu}_e]\!]$ be the corresponding jump across e. Then we define the approximate flux vector as $\widetilde{\boldsymbol{\sigma}}_h := \vartheta(\phi_h)\nabla\phi_h - \phi_h \boldsymbol{q}_h - b(\phi_h)\boldsymbol{k}$ and define an element-wise local error indicator associated to a semidiscretization of (4-2)–(4-3) as follows:

$$\begin{aligned}\theta_K^2 :=& \|\boldsymbol{f}\phi_h - (\partial_t \boldsymbol{q}_h - \mathbf{div}\boldsymbol{\sigma}_h)\|_{0,K}^2 + \left\|\nabla \boldsymbol{q}_h - (\mu(\phi_h))^{-1}\boldsymbol{\sigma}_h^{\mathrm{d}}\right\|_{0,K}^2 \\ &+ h_K^2 \|g - (\partial_t \phi_h - \mathrm{div}\widetilde{\boldsymbol{\sigma}}_h)\|_{0,K}^2 + h_K^2 \left\|\mathbf{curl}\left((\mu(\phi_h))^{-1}\boldsymbol{\sigma}_h^{\mathrm{d}}\right)\right\|_{0,K}^2 \\ &+ \sum_{e\in\mathcal{E}(K)} h_e \left(\left\| [\![(\mu(\phi_h))^{-1}\boldsymbol{\sigma}_h^{\mathrm{d}}\boldsymbol{s}_e]\!] \right\|_{0,e}^2 + \|[\![\widetilde{\boldsymbol{\sigma}}_h \cdot \boldsymbol{\nu}_e]\!]\|_{0,e}^2 \right) + \sum_{e\in\mathcal{E}^{\Gamma_D}(K)} \|\boldsymbol{q}_D - \boldsymbol{q}_h\|_{0,e}^2 \\ &+ \sum_{e\in\mathcal{E}^{\Gamma_N}(K)} h_e \|\widetilde{\boldsymbol{\sigma}}_h \cdot \boldsymbol{\nu}_e\|_{0,e}^2 + \sum_{e\in\mathcal{E}^{\Gamma_D}(K)} h_e \left\| \frac{\mathrm{d}\boldsymbol{q}_D}{\mathrm{d}s_e} - (\mu(\phi_h))^{-1}\boldsymbol{\sigma}_h^{\mathrm{d}}\boldsymbol{s}_e \right\|_{0,e}^2 .\end{aligned}$$

A global residual error estimator can then be defined as $\boldsymbol{\theta} := \{\sum_{K\in\mathcal{T}_h} \theta_K^2\}^{1/2}$, which has resemblance to the first residual-based indicator proposed in Alvarez, Gatica, and Ruiz-Baier [2017], and which has been shown to be efficient and reliable.

4.4 Numerical example. Let us consider a zeolite suspension in a secondary clarifier unit, where domain configuration and dimensions are taken from the Eindhoven WWTP (see Figure 10), and whose geometry is precisely described in Bürger, Kumar, and Ruiz-Baier [2015]. A numerical simulation using axisymmetric discontinuous FVE schemes for primal formulations has been developed in Bürger, Kumar, and Ruiz-Baier [ibid.]. We use the model parameters of that study, but here stating the set of equations in mixed form (4-2) and employ a lowest-order mixed-primal scheme as the one proposed in Alvarez, Gatica, and Ruiz-Baier [2016b]. A backward Euler method is used for the time discretization setting a fixed timestep of $\Delta t = 5\,\mathrm{s}$ and the system is evolved until $t_{\mathrm{final}} = 12000\mathrm{s}$. The device features a feed inlet Γ_{in} and a peripheral overflow annular region Γ_{ofl}. A suspension is injected through Γ_{in} with constant velocity $\boldsymbol{q}_{\mathrm{in}} = (0, 0.17)^T$ and having a concentration of $\phi = 0.08$. On Γ_{out} we set $\boldsymbol{q}_{\mathrm{out}} = (0, -1.5\mathrm{e}^6)^T$ and on Γ_{ofl} we impose zero normal Cauchy stresses; and on the remainder of $\partial\Omega$ we prescribe $\boldsymbol{q} = \mathbf{0}$ and no-flux conditions for ϕ.

The remaining parameters are chosen as $\sigma_e'(\phi) = (\sigma_0\alpha/\phi_c^\alpha)\phi^{\alpha-1}$, $\sigma_0 = 0.22\,\mathrm{Pa}$, $\alpha = 5$, $\beta = 2.5$, $\rho_L = 998.2\,\mathrm{kg/m^3}$, $\rho_X = 1750\,\mathrm{kg/m^3}$, $\phi_c = 0.014$, $\tilde{\phi}_{\max} = 0.95$, $v_\infty = 0.0028935\,\mathrm{m/s}$, $g = 9.8\,\mathrm{m/s^2}$, and $D_0 = 0.0028935\,\mathrm{m^2/s}$. The physical bounds for the concentration imply that the stabilisation parameters needed for the augmented mixed-primal FE method take the values $\kappa_1 = 0.256$ and $\kappa_2 = 0.25$.

We implement an adaptive mesh refinement strategy according to the a posteriori error indicator $\boldsymbol{\theta}$, which we invoke at the end of each time step. The marking-refining algorithm is based on the equi-distribution of the error indicators in such a way that the diameter of each new element (contained in a generic element K on the initial coarse mesh) is proportional to the initial diameter times the ratio $\bar{\boldsymbol{\theta}}_h/\eta_K$, where $\bar{\boldsymbol{\theta}}_h$ is the mean value of $\boldsymbol{\theta}$ over the initial mesh (Verfürth [1996]). On each time step we then solve the coupled set of nonlinear equations using a fixed point method, stopping the Picard iterations when a residual tolerance of 1e-6 is attained. Inside each fixed-point step we solve the discretized mixed Stokes equations with a preconditioned BiCGStab method, and a nested Newton solver is employed for the nonlinear transport equation using the same value for the residual tolerance as stopping criterion and the same solver for the corresponding linear systems.

Figure 11 (top rows) presents snapshots of the numerically computed concentration profiles on a surface line integration visualization of the velocity field. We observe velocity patterns avoiding the skirt baffle and the accumulation of sediment on the bottom of the tank. The sequence of refined meshes indicates that the a posteriori error estimator identifies the zones of high concentration gradients and marked flow features. A cluster of elements is formed near these particular zones.

4.5 Ongoing extensions. The theory exposed above still does not cover the analysis of flow coupled to degenerate elliptic or parabolic equations, that is when the diffusivity vanishes for all concentrations below a critical value ϕ_c, invalidating the fundamental assumptions of strong ellipticity and monotonicity that permits the derivation of solvability and stability of continuous and discrete problems. Then the classical tools employed in the continuous analysis as well as in the construction and analysis of the associated numerical method (Alvarez, Gatica, and Ruiz-Baier [2015, 2016b,a], Bürger, Kumar, and Ruiz-Baier [2015], Bürger, Kumar, Kenettinkara, and Ruiz-Baier [2016], Bürger, Ruiz-Baier, and Torres [2012], and Ruiz-Baier and Torres [2015]), need to be extended. Part of such a theoretical formalism has been around for many years in the context of hyperbolic conservation laws (*cf.* Andreianov, Karlsen, and Risebro [2011] and Berres, Bürger, Karlsen, and Tory [2003] and the references therein), but has not yet been exploited in multidimensional models of sedimentation. These developments will need to encompass entropy solutions, low-regularity finite element discretizations, discontinuous FVE, and non-conforming methods. It is also left to investigate the performance of a posteriori error indicators developed for FVE schemes applied to (4-1), where sample preliminary studies include the case of convection-reaction-diffusion (Lazarov and Tomov [2002]).

References

Mario Alvarez, Gabriel N. Gatica, and Ricardo Ruiz-Baier (2015). "An augmented mixed-primal finite element method for a coupled flow-transport problem". *ESAIM Math. Model. Numer. Anal.* 49.5, pp. 1399–1427. MR: 3423229 (cit. on pp. 3488, 3489, 3491).

– (2016a). "A mixed-primal finite element approximation of a sedimentation-consolidation system". *Math. Models Methods Appl. Sci.* 26.5, pp. 867–900. MR: 3464424 (cit. on p. 3491).

– (2016b). "*A posteriori* error analysis for a viscous flow-transport problem". *ESAIM Math. Model. Numer. Anal.* 50.6, pp. 1789–1816. MR: 3580122 (cit. on pp. 3489–3491).

– (2017). "A posteriori error estimation for an augmented mixed-primal method applied to sedimentation-consolidation systems". CI^{2}MA preprint (cit. on pp. 3489, 3490).

Boris Andreianov, Kenneth Hvistendahl Karlsen, and Nils Henrik Risebro (2011). "A theory of L^1-dissipative solvers for scalar conservation laws with discontinuous flux". *Arch. Ration. Mech. Anal.* 201.1, pp. 27–86. MR: 2807133 (cit. on p. 3491).

Georg Anestis (1981). "Eine eindimensionale Theorie der Sedimentation in Absetzbehältern veränderlichen Querschnitts und in Zentrifugen". PhD thesis. TU Vienna, Austria (cit. on pp. 3478–3480).

Randolph E. Bank and Donald J. Rose (1987). "Some error estimates for the box method". *SIAM J. Numer. Anal.* 24.4, pp. 777–787. MR: 899703 (cit. on p. 3489).

Stefan Berres, Raimund Bürger, Kenneth H. Karlsen, and Elmer M. Tory (2003). "Strongly degenerate parabolic-hyperbolic systems modeling polydisperse sedimentation with compression". *SIAM J. Appl. Math.* 64.1, pp. 41–80. MR: 2029124 (cit. on p. 3491).

Fernando Betancourt, Raimund Bürger, Ricardo Ruiz-Baier, Héctor Torres, and Carlos A. Vega (2014). "On numerical methods for hyperbolic conservation laws and related equations modelling sedimentation of solid-liquid suspensions". In: *Hyperbolic conservation laws and related analysis with applications*. Vol. 49. Springer Proc. Math. Stat. Springer, Heidelberg, pp. 23–68. MR: 3111126 (cit. on pp. 3475, 3488).

Malte Braack and Thomas Richter (2007). "Solving multidimensional reactive flow problems with adaptive finite elements". In: *Reactive flows, diffusion and transport*. Springer, Berlin, pp. 93–112. MR: 2275759 (cit. on p. 3489).

Miroslav Bulíček and Petra Pustějovská (2014). "Existence analysis for a model describing flow of an incompressible chemically reacting non-Newtonian fluid". *SIAM J. Math. Anal.* 46.5, pp. 3223–3240. MR: 3262601 (cit. on p. 3489).

Raimund Bürger, Julio Careaga, and Stefan Diehl (n.d.). "Flux identification of scalar conservation laws from sedimentation in a cone". *IMA J. Appl. Math.* in press () (cit. on pp. 3481–3484).

– (2017). "Entropy solutions of a scalar conservation law modeling sedimentation in vessels with varying cross-sectional area". *SIAM J. Appl. Math.* 77.2, pp. 789–811. MR: 3640636 (cit. on pp. 3478, 3479, 3481, 3482).

Raimund Bürger, Julio Careaga, Stefan Diehl, Camilo Mejías, Ingmar Nopens, Elena Torfs, and Peter A Vanrolleghem (2016). "Simulations of reactive settling of activated sludge with a reduced biokinetic model". *Computers & Chemical Engineering* 92, pp. 216–229 (cit. on pp. 3476, 3484, 3500).

Raimund Bürger, Julio Careaga, Stefan Diehl, Ryan Merckel, and Jesús Zambrano (n.d.). *Estimating the hindered-settling flux function from a batch test in a cone*. Submitted (cit. on pp. 3478, 3484).

Raimund Bürger and Stefan Diehl (2013). "Convexity-preserving flux identification for scalar conservation laws modelling sedimentation". *Inverse Problems* 29.4, pp. 045008, 30. MR: 3042084 (cit. on pp. 3475, 3483, 3484).

Raimund Bürger, Stefan Diehl, and Camilo Mejías (n.d.). *A difference scheme for a degenerating convection-diffusion-reaction system modelling continuous sedimentation* (cit. on pp. 3475, 3476, 3484–3486).

Raimund Bürger, Stefan Diehl, and Ingmar Nopens (2011). "A consistent modelling methodology for secondary settling tanks in wastewater treatment". *Water Research* 45.6, pp. 2247–2260 (cit. on p. 3476).

Raimund Bürger, Kenneth H. Karlsen, and John D. Towers (2005). "A model of continuous sedimentation of flocculated suspensions in clarifier-thickener units". *SIAM J. Appl. Math.* 65.3, pp. 882–940. MR: 2136036 (cit. on pp. 3474, 3476, 3485, 3486).

Raimund Bürger, Kenneth Hvistendahl Karlsen, Nils Henrik Risebro, and John D. Towers (2004). "Well-posedness in BV_t and convergence of a difference scheme for continuous sedimentation in ideal clarifier-thickener units". *Numer. Math.* 97.1, pp. 25–65. MR: 2045458 (cit. on p. 3486).

Raimund Bürger, Sarvesh Kumar, Sudarshan Kumar Kenettinkara, and Ricardo Ruiz-Baier (2016). "Discontinuous approximation of viscous two-phase flow in heterogeneous porous media". *J. Comput. Phys.* 321, pp. 126–150. MR: 3527561 (cit. on pp. 3489, 3491).

Raimund Bürger, Sarvesh Kumar, and Ricardo Ruiz-Baier (2015). "Discontinuous finite volume element discretization for coupled flow-transport problems arising in models of sedimentation". *J. Comput. Phys.* 299, pp. 446–471. MR: 3384736 (cit. on pp. 3489–3491).

Raimund Bürger, Chun Liu, and Wolfgang L. Wendland (2001). "Existence and stability for mathematical models of sedimentation-consolidation processes in several space dimensions". *J. Math. Anal. Appl.* 264.2, pp. 288–310. MR: 1876734 (cit. on p. 3488).

Raimund Bürger, Ricardo Ruiz-Baier, and Héctor Torres (2012). "A stabilized finite volume element formulation for sedimentation-consolidation processes". *SIAM J. Sci. Comput.* 34.3, B265–B289. MR: 2970279 (cit. on pp. 3489, 3491).

Raimund Bürger, Ricardo Ruiz, Kai Schneider, and Mauricio Sepúlveda (2008). "Fully adaptive multiresolution schemes for strongly degenerate parabolic equations in one space dimension". *M2AN Math. Model. Numer. Anal.* 42.4, pp. 535–563. MR: 2437773 (cit. on p. 3489).

Raimund Bürger, Wolfgang L. Wendland, and Fernando Concha (2000). "Model equations for gravitational sedimentation-consolidation processes". *ZAMM Z. Angew. Math. Mech.* 80.2, pp. 79–92. MR: 1742180 (cit. on p. 3487).

Caterina Calgaro, Emmanuel Creusé, and Thierry Goudon (2008). "An hybrid finite volume-finite element method for variable density incompressible flows". *J. Comput. Phys.* 227.9, pp. 4671–4696. MR: 2406553 (cit. on p. 3489).

Eligio Colmenares, Gabriel N. Gatica, and Ricardo Oyarzúa (2016). "Analysis of an augmented mixed-primal formulation for the stationary Boussinesq problem". *Numer. Methods Partial Differential Equations* 32.2, pp. 445–478. MR: 3454217 (cit. on p. 3489).

Christopher Cox, Hyesuk Lee, and David Szurley (2007). "Finite element approximation of the non-isothermal Stokes-Oldroyd equations". *Int. J. Numer. Anal. Model.* 4.3-4, pp. 425–440. MR: 2344050 (cit. on p. 3489).

Stefan Diehl (1997). "Continuous sedimentation of multi-component particles". *Math. Methods Appl. Sci.* 20.15, pp. 1345–1364. MR: 1474212 (cit. on p. 3485).

– (2007). "Estimation of the batch-settling flux function for an ideal suspension from only two experiments". *Chemical Engineering Science* 62.17, pp. 4589–4601 (cit. on pp. 3483, 3484).

– (2012). "Shock-wave behaviour of sedimentation in wastewater treatment: a rich problem". In: *Analysis for science, engineering and beyond*. Vol. 6. Springer Proc. Math. Springer, Heidelberg, pp. 175–214. MR: 3288029 (cit. on p. 3475).

– (2015). "Numerical identification of constitutive functions in scalar nonlinear convection-diffusion equations with application to batch sedimentation". *Appl. Numer. Math.* 95, pp. 154–172. MR: 3349692 (cit. on p. 3476).

George A. Ekama, James L. Barnard, F. Wolfgang Günthert, Peter Krebs, J. Alex McCorquodale, Denny S. Parker, and Eric J. Wahlberg (1997). *Secondary Settling Tanks-Theory, Modeling, Design and Operation*. Tech. rep. International Association on Water Quality, London (cit. on p. 3488).

Richard Ewing, Raytcho Lazarov, and Yanping Lin (2000). "Finite volume element approximations of nonlocal reactive flows in porous media". *Numer. Methods Partial Differential Equations* 16.3, pp. 285–311. MR: 1752414 (cit. on p. 3489).

M. Farhloul and A. Zine (2011). "A dual mixed formulation for non-isothermal Oldroyd-Stokes problem". *Math. Model. Nat. Phenom.* 6.5, pp. 130–156. MR: 2825226 (cit. on p. 3489).

Mogens Henze, C.P. Leslie Grady, Willi Gujer, Gerrit v.R. Marais, and Tomonori Matsuo (1987). Tech. rep. International Association on Water Quality, London (cit. on pp. 3485, 3500).

Helge Holden and Nils Henrik Risebro (2015). *Front tracking for hyperbolic conservation laws*. Second. Vol. 152. Applied Mathematical Sciences. Springer, Heidelberg, pp. xiv+515. MR: 3443431 (cit. on pp. 3479, 3480).

K. H. Karlsen, N. H. Risebro, and J. D. Towers (2002). "Upwind difference approximations for degenerate parabolic convection-diffusion equations with a discontinuous coefficient". *IMA J. Numer. Anal.* 22.4, pp. 623–664. MR: 1937244 (cit. on p. 3486).

Arzhang Khalili, A.J. Basu, Uwe Pietrzyk, and Bo Barker Jørgensen (1999). "Advective transport through permeable sediments: a new numerical and experimental approach". *Acta Mechanica* 132.1-4, pp. 221–227 (cit. on p. 3488).

Sarvesh Kumar and Ricardo Ruiz-Baier (2015). "Equal order discontinuous finite volume element methods for the Stokes problem". *J. Sci. Comput.* 65.3, pp. 956–978. MR: 3417268 (cit. on p. 3489).

Matthias Kunik (1993). "A solution formula for a nonconvex scalar hyperbolic conservation law with monotone initial data". *Math. Methods Appl. Sci.* 16.12, pp. 895–902. MR: 1247889 (cit. on pp. 3483, 3484).

George J Kynch (1952). "A theory of sedimentation". *Transactions of the Faraday society* 48, pp. 166–176 (cit. on pp. 3474, 3483).

Mats G. Larson, Robert Söderlund, and Fredrik Bengzon (2008). "Adaptive finite element approximation of coupled flow and transport problems with applications in heat transfer". *Internat. J. Numer. Methods Fluids* 57.9, pp. 1397–1420. MR: 2435098 (cit. on p. 3489).

Raytcho Lazarov and Stanimire Tomov (2002). "A posteriori error estimates for finite volume element approximations of convection-diffusion-reaction equations". *Comput. Geosci.* 6.3-4. Locally conservative numerical methods for flow in porous media, pp. 483–503. MR: 1956027 (cit. on p. 3491).

Alfio Quarteroni and Ricardo Ruiz-Baier (2011). "Analysis of a finite volume element method for the Stokes problem". *Numer. Math.* 118.4, pp. 737–764. MR: 2822498 (cit. on p. 3489).

Rekha R Rao, Lisa A Mondy, and Stephen A Altobelli (2007). "Instabilities during batch sedimentation in geometries containing obstacles: A numerical and experimental study". *International Journal for Numerical Methods in Fluids* 55.8, pp. 723–735 (cit. on p. 3488).

Ricardo Ruiz-Baier and Ivan Lunati (2016). "Mixed finite element–discontinuous finite volume element discretization of a general class of multicontinuum models". *J. Comput. Phys.* 322, pp. 666–688. MR: 3534882 (cit. on p. 3488).

Ricardo Ruiz-Baier and Héctor Torres (2015). "Numerical solution of a multidimensional sedimentation problem using finite volume-element methods". *Appl. Numer. Math.* 95, pp. 280–291. MR: 3349700 (cit. on pp. 3489, 3491).

Rüdiger Verfürth (1996). *A review of a posteriori error estimation and adaptive mesh-refinement techniques*. Wiley-Teubner (Chichester) (cit. on p. 3491).

Juan Wen, Yinnian He, and Jianhong Yang (2013). "Multiscale enrichment of a finite volume element method for the stationary Navier-Stokes problem". *Int. J. Comput. Math.* 90.9, pp. 1938–1957. MR: 3171872 (cit. on p. 3489).

Received 2017-11-30.

Raimund Bürger
CI^{2}MA and Departamento de Ingeniería Matemática
Universidad de Concepción
Casilla 160-C, Concepción
Chile
rburger@ing-mat.udec.cl

Julio Careaga
Centre for Mathematical Sciences
Lund University
P.O. Box 118
S-221 00 Lund
Sweden
julio.careaga@math.lth.se

Stefan Diehl
Centre for Mathematical Sciences
Lund University
P.O. Box 118
S-221 00 Lund
Sweden
stefan.diehl@math.lth.se

Camilo Mejías
CI^{2}MA and Departamento de Ingeniería Matemática
Universidad de Concepción
Casilla 160-C, Concepción
Chile
cmejias@ing-mat.udec.cl

Ricardo Ruiz Baier

Mathematical Institute
Oxford University
Andrew Wiles Building
Woodstock Road
OX2 6GG Oxford
UK
ruizbaier@maths.ox.ac.uk

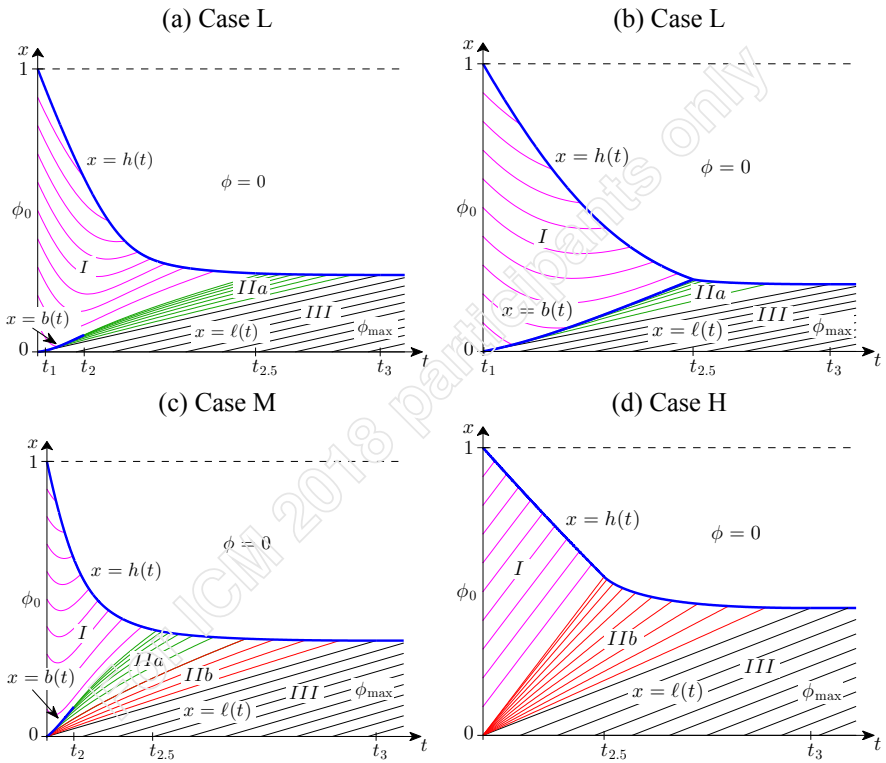

Figure 5: Solutions of (2-1) in a truncated cone ($q = 1/2$, $p > 0$) with f given by (1-6): (a) Case L, $r_V = 4$, $\phi_0 = 0.04$, $p = 1/18$; (b) Case L, $r_V = 4$, $\phi_0 = 0.1$, $p = 1/3$; (c) Case M, $r_V = 5$, $\phi_0 = 0.12$, $p = 1/6$; (d) Case H, $r_V = 4.7$, $\phi_0 = 0.43$, $p = 9.5$. The solid blue curves are discontinuities.

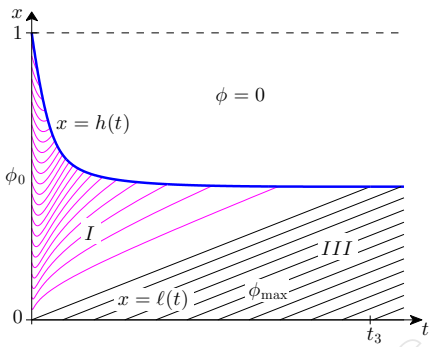

Figure 6: Solution corresponding to item (i) of Theorem 2.2.

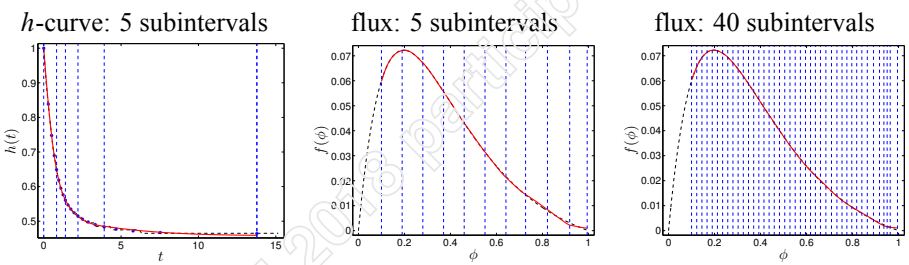

Figure 7: Flux identification via settling in a cone with $\phi_0 = 0.1$ from synthetic data of the discontinuity $x = h(t)$. The number of subintervals is that of cubic polynomials used for the h-curve. The true flux is shown in dashed and the identified fluxes in solid red.

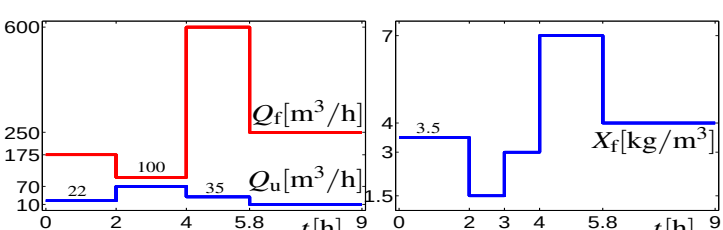

Figure 8: Piecewise constant functions Q_f and Q_u (feed and underflow volume rates) and X_f (solids feed concentration) for the numerical example of reactive settling (Figure 9).

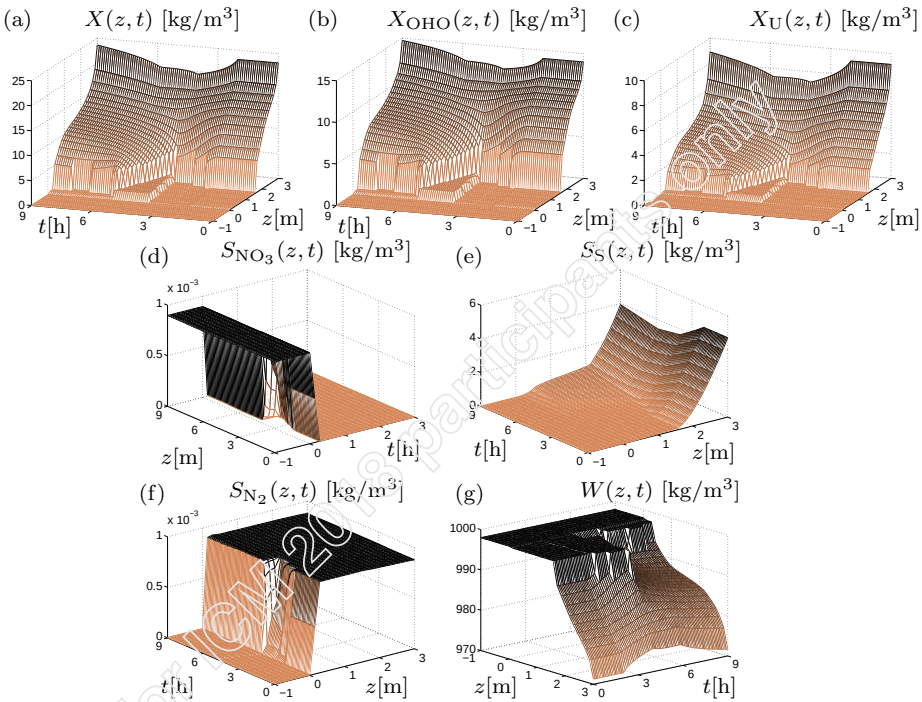

Figure 9: Simulation of reactive settling (denitrification) in an SST under variations of Q_{u}, Q_{f} and X_{f} (see Figure 8). Constants are standard in ASM1 (Henze, Grady, Gujer, Marais, and Matsuo [1987]) or arise in a strongly reduced model (Bürger, Careaga, Diehl, Mejías, Nopens, Torfs, and Vanrolleghem [2016]): $b = 6.94 \times 10^{-6}\,\mathrm{s}^{-1}$, $f_{\mathrm{p}} = 0.2$, $K_{\mathrm{NO_3}} = 5.0 \times 10^{-4}\,\mathrm{kg\,m}^{-3}$, $X_{\max} = 30\,\mathrm{kg\,m}^{-3}$, (the maximum solids concentration), $\mu_{\max} = 5.56 \times 10^{-5}\,\mathrm{s}^{-1}$, $v_0 = 1.76 \times 10^{-3}\,\mathrm{m\,s}^{-1}$, $\rho_X = 1050\,\mathrm{kg\,m}^{-3}$, $\rho_L = 998\,\mathrm{kg\,m}^{-3}$, $g = 9.8\,\mathrm{m\,s}^{-2}$ (acceleration of gravity) and $Y = 0.67$ (yield factor).

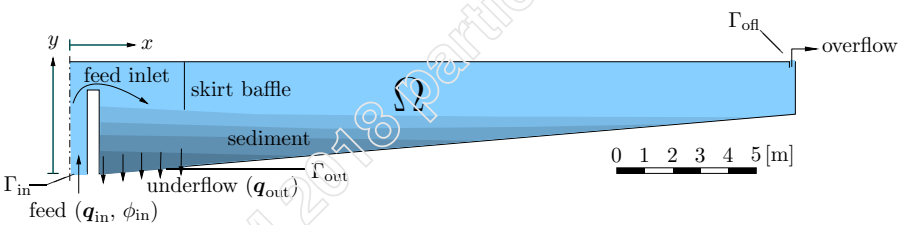

Figure 10: Settling tank from Eindhoven WWTP.

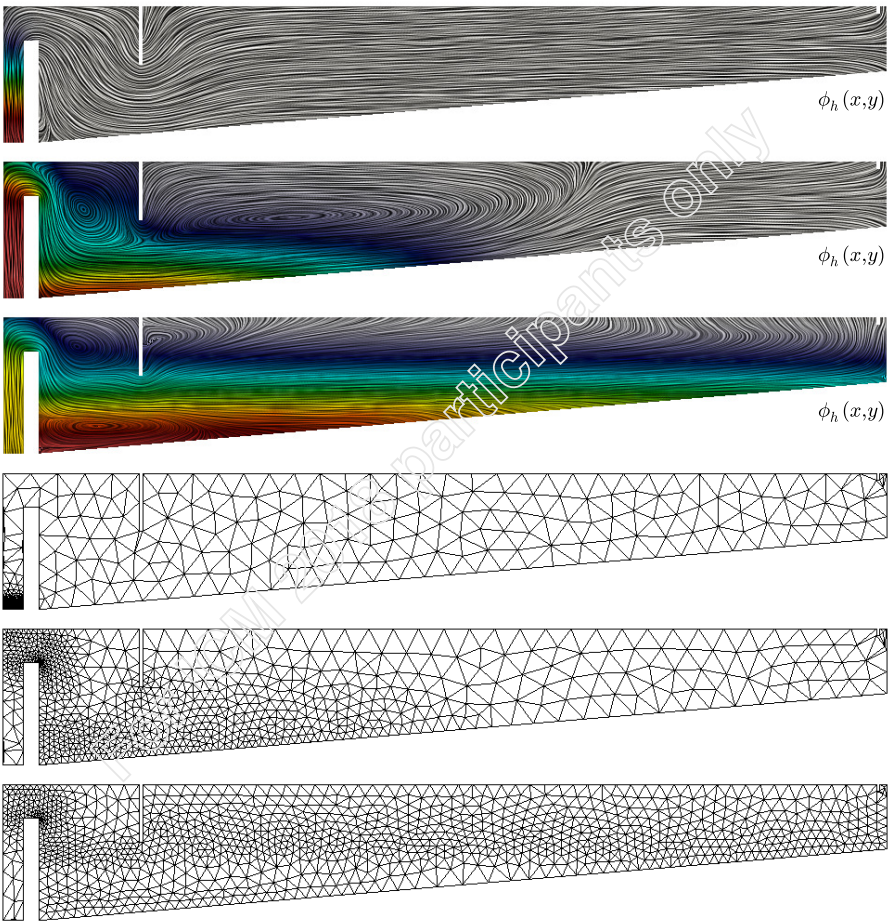

Figure 11: Example: Mixed-primal FE approximation of ϕ at $t = 200$ s, $t = 4000$ s, and $t = 12000$ s, and corresponding adapted meshes refined using the a posteriori error estimator $\boldsymbol{\theta}$.